Progress In Electromagnetics Research, Vol. 170, 177–186, 2021

Surface Electromagnetic Waves at Gradual Interfaces between Lossy Media

Igor I. Smolyaninov[1, 2, *]

Abstract—A low loss propagating electromagnetic wave is shown to exist at a gradual interface between two lossy conductive media. Such a surface wave may be guided by a seafloor-seawater interface, and it may be used in radio communication and imaging underwater. It should allow communication distances of the order of 500 m at 10 kHz along a sandy seabed. Similar surface waves may also be guided by various tissue boundaries inside a human body. For example, such surface wave solutions may exist at planar interfaces between skull bones and grey matter inside a human head at 6 GHz.

1. INTRODUCTION

Sharp step-like planar interfaces between media having different electromagnetic properties (see Fig. 1(a)) are known to sometimes support surface electromagnetic waves (SEW) [1–6]. However, long-range low-loss propagation of such SEWs is known to occur only in some limited circumstances. The most well-known cases of such low-loss SEWs include surface plasmons (SP), which propagate along metal-dielectric interfaces [7], and Zenneck waves [8], which may propagate along interfaces between highly lossy conductive media and low-loss dielectrics. In both cases, the wave vector k of such SEWs along the interface may be determined as:

$$k = \frac{\omega}{c}\left(\frac{\varepsilon_1\varepsilon_2}{\varepsilon_1+\varepsilon_2}\right)^{1/2} \tag{1}$$

where ε_1 and ε_2 are complex dielectric permittivities of the adjacent media, resulting in $\mathrm{Im}(k) \ll \mathrm{Re}(k)$ for both SPs and Zenneck waves [7, 8]. Indeed, besides the trivial case when both ε_1 and ε_2 are mostly real and positive, Eq. (1) may produce an almost purely real answer if $\mathrm{Re}(\varepsilon_1)$ and $\mathrm{Re}(\varepsilon_2)$ have opposite signs, $\mathrm{Re}(\varepsilon_1+\varepsilon_2) < 0$, and the imaginary parts of both dielectric permittivities are small. This case corresponds to an SP wave at a metal-dielectric interface. Another possibility may be the case when $\mathrm{Im}(\varepsilon_1) \gg \mathrm{Re}(\varepsilon_2)$, which corresponds to the Zenneck wave at an interface between a highly lossy conductive medium and a good dielectric. However, in the latter case the resulting wave vector appears smaller than the wave vector of regular photons in the dielectric, which leads to the "leaky" characteristic of this surface wave: while it should be able to propagate over a perfectly smooth interface, surface imperfections must strongly scatter the Zenneck waves into photons propagating inside the dielectric. The electromagnetic properties of interfaces between two media having different dielectric permittivities may also be characterized using impedance matching networks [9–16], which produces similar results.

In this paper, I will consider a more general situation in which the dielectric permittivity (or conductivity) of a medium changes continuously and gradually across an interface, as illustrated in Fig. 1(b). It appears that new kinds of SEW solutions may exist in such situations. We will demonstrate that a relatively low loss propagating SEW may exist at a gradual interface between two highly lossy

Received 30 April 2021, Accepted 1 June 2021, Scheduled 3 June 2021

* Corresponding author: Igor I. Smolyaninov (igor.smolyaninov@saltenna.com).

[1] The Saltenna LLC, 1751 Pinnacle Drive, Suite 600 McLean, VA 22102-4903, USA. [2] University of Maryland, USA.

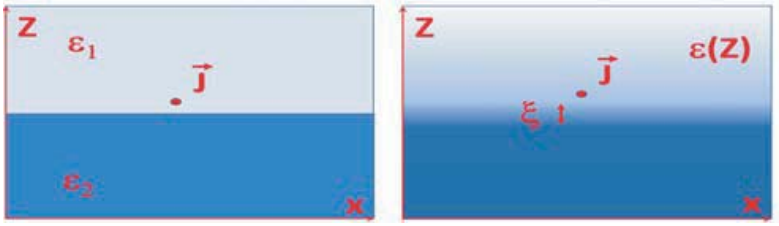

(a) (b)

Figure 1. (a) Conventional sharp step-like geometry of the SEW problem considered in [1–8]. A current line source is located above the sharp interface. (b) Gradual interface problem considered in this paper. The dielectric permittivity of the medium ε is continuous and it depends only on z coordinate, which is illustrated by halftones. The gradual transition layer thickness between the two media equals ξ.

conductive media. While this analysis is applicable to any frequency range, this work is primarily motivated by recent experimental progress in underwater radio communication [17] and potential application of our analysis in bioelectromagnetics.

2. THEORETICAL CONSIDERATION

Let us solve macroscopic Maxwell equations in a non-magnetic ($\mu = 1$) medium, in which the dielectric permittivity is continuous, and it depends on z coordinate only: $\varepsilon = \varepsilon(z)$, as shown in Fig. 1(b).

For time harmonic fields proportional to $e^{-i\omega t}$, the macroscopic Maxwell equations may be written as

$$\vec{\nabla} \cdot \vec{D} = 0, \quad \vec{\nabla} \cdot \vec{B} = 0, \quad \vec{\nabla} \times \vec{E} = i\omega \vec{B}, \quad \text{and} \quad \vec{\nabla} \times \vec{H} = \vec{J} - i\omega \vec{D} \tag{2}$$

which leads to a wave equation with a current line source term:

$$\vec{\nabla} \times \left(\vec{\nabla} \times \vec{E} \right) - \frac{\omega^2 \varepsilon}{c^2} \vec{E} = i\omega \mu_0 \vec{J} \tag{3}$$

After straightforward transformations, this wave equation may be rewritten as

$$-\nabla^2 \vec{E} - \vec{\nabla} \left(E_z \frac{\partial \varepsilon}{\varepsilon \partial z} \right) - \frac{\varepsilon \omega^2}{c^2} \vec{E} = i\omega \mu_0 \vec{J} \tag{4}$$

It is well known in the electromagnetic theory that the field generated by the source is obtained as a superposition of propagating source-free electromagnetic modes traveling outward from the source. These propagating electromagnetic waves are found as solutions of the source-free homogeneous Maxwell equations. Therefore, for the sake of simplicity, and since we are interested only in the surface modes, let us search for a source-free electromagnetic wave propagating in the x direction, so that its field is proportional to $e^{i(kx-\omega t)}$. Depending on the polarization state (TE or TM) of the electromagnetic wave solution, Eq. (4) with a zero source term may be rewritten in the form of the following effective Schrodinger equations:

$$-\frac{\partial^2 E_y}{\partial z^2} - \frac{\varepsilon(z)\omega^2}{c^2} E_y = -k^2 E_y \tag{5}$$

for the TE polarized wave (in which $E_z = 0$), and

$$-\frac{\partial^2 E_z}{\partial z^2} - \frac{\partial E_z}{\partial z} \frac{\partial \ln \varepsilon}{\partial z} - \left(\frac{\varepsilon(z)\omega^2}{c^2} + \frac{\partial^2 \ln \varepsilon}{\partial z^2} \right) E_z = -k^2 E_z \tag{6}$$

for the TM polarized wave (in which $E_z \neq 0$). Eq. (6) may be further transformed by introducing the effective wave function ψ as $E_z = \psi / \varepsilon^{1/2}$ which leads to

$$-\frac{\partial^2 \psi}{\partial z^2} + \left(-\frac{\varepsilon(z)\omega^2}{c^2} - \frac{1}{2} \frac{\partial^2 \varepsilon}{\varepsilon \partial z^2} + \frac{3}{4} \frac{\left(\partial \varepsilon / \partial z \right)^2}{\varepsilon^2} \right) \psi = -\frac{\partial^2 \psi}{\partial z^2} + V\psi = -k^2 \psi \tag{7}$$

for the TM polarized wave. In both cases (Eq. (5) for the TE wave and Eq. (7) for the TM wave), $-k^2$ plays the role of effective energy in the respective Schrodinger equations. However, the effective potential energies in the TE and TM cases are different. In the TE case, the effective potential energy is $V(z) = -\frac{\varepsilon(z)\omega^2}{c^2}$, so that the only solutions of Eq. (5) having propagating characteristic ($\mathrm{Im}(k) \ll \mathrm{Re}(k)$) are those which behave like guided modes in a waveguide-like distribution of $\varepsilon = \varepsilon(z)$ (in which the dielectric permittivity is positive and almost purely real), and Eq. (5) does not have SEW solutions.

Let us now study the TM-polarized solutions of Eq. (7). In agreement with the well-known SEW physics [7, 8], surface plasmon and Zenneck SEW solutions do appear in this case due to the presence of derivative terms in the effective potential energy. For example, the $\frac{3}{4}\frac{(\partial\varepsilon/\partial z)^2}{\varepsilon^2}$ term dominates the potential energy expression in Eq. (7) when $\mathrm{Re}(\varepsilon)$ gradually passes through zero at the metal-dielectric interface, leading to the appearance of surface plasmon SEW solutions. Indeed, this term becomes negative and strongly attractive whenever $\mathrm{Re}(\varepsilon(z))$ passes through zero:

$$V(z) \approx \frac{3}{4}\frac{(\partial\varepsilon/\partial z)^2}{\varepsilon^2} \approx -\frac{3}{4}\frac{(\partial\mathrm{Re}(\varepsilon)/\partial z)^2}{\mathrm{Im}(\varepsilon)^2} \tag{8}$$

The same term starts to dominate $V(z)$ at the very top of the transition layer between a highly lossy conductive medium and air, leading to the appearance of Zenneck wave solution. However, careful examination of the effective potential energy expression in the TM case

$$V(z) = -\frac{4\pi^2\varepsilon(z)}{\lambda_0^2} - \frac{1}{2}\frac{\partial^2\varepsilon}{\varepsilon\partial z^2} + \frac{3}{4}\frac{(\partial\varepsilon/\partial z)^2}{\varepsilon^2} \tag{9}$$

(where λ is the free space wavelength) reveals other situations which lead to novel propagating SEW solutions having $\mathrm{Im}(k) \ll \mathrm{Re}(k)$. Let us consider a gradual interface between two media, which have approximately the same loss angle δ, and let us assume that the loss tangent remains approximately constant across the transition layer ξ between these media (see Fig. 1(b)):

$$\varepsilon(z) = a(z)e^{i\delta}, \tag{10}$$

where $a(z)$ is the z-dependent magnitude of the dielectric permittivity. Under these assumptions, the effective potential in the TM case (since $\omega = 2\pi c/\lambda_0$) equals

$$V(z) = -\frac{4\pi^2 a(z)e^{i\delta}}{\lambda_0^2} - \frac{1}{2}\frac{\partial^2 a}{a\partial z^2} + \frac{3}{4}\frac{(\partial a/\partial z)^2}{a^2}. \tag{11}$$

If the spatial scale ξ is much smaller than λ, the second and third terms will dominate in Eq. (11), and since these terms are real, $\mathrm{Im}(V) \ll \mathrm{Re}(V)$. The resulting potential well will be deep enough, so that the wave vector of the resulting surface wave solution will be very large ($k \sim 1/\xi \gg 2\pi/\lambda_0$), and this novel SEW will have propagating characteristic ($\mathrm{Im}(k) \ll \mathrm{Re}(k)$). These conclusions will be confirmed by detailed numerical simulations performed in Section 3.

Note that a 1D Schrodinger equation describing a one-dimensional potential well of an arbitrary shape always has at least one eigenstate [18]. SEW solutions are tightly localized near the interface. Indeed, based on Eq. (7), far from the interface where $V \to 0$ its electric field attenuates as $E_z \sim e^{-kz}$ away from the interface inside both media. On the other hand, in the opposite limit when ξ is comparable to or larger than λ_0, the newly found SEW solution disappears since the first term will dominate in Eq. (11). This observation gives us the high frequency limit on SEW existence at a given fixed dielectric permittivity gradient.

Another necessary condition of SEW existence established above is the approximate constancy of the loss angle δ across the interface. Otherwise, the $\mathrm{Im}(V) \ll \mathrm{Re}(V)$ condition will be violated, and the SEW solution given by Eq. (7) will not have propagating characteristic. This condition gives us the limits on the frequency bands in which the newly found SEW solution may potentially exist for a given combination of the bounding media. The loss angle δ must remain approximately constant for both media within the limits of such a band.

3. RESULTS OF NUMERICAL SIMULATIONS AND DISCUSSION

3.1. Surface Wave Propagation along the Seawater-Seabed Interface

Let us confirm the analytical theoretical consideration above by detailed simulations in two situations of practical importance. First, let us analyze propagation of the newly found SEWs along the seawater-seabed interface and demonstrate that they may be used in long-distance underwater radio communication. The sandy seabed conductivity of $\sigma = 1\,\mathrm{S/m}$ has been measured in [19], while the average conductivity of seawater is typically assumed to be $\sigma = 4\,\mathrm{S/m}$ [17]. In the ELF-VHF radio frequency ranges, the dielectric permittivities of seawater and sandy seabed are defined by their conductivities:

$$\varepsilon \approx i\varepsilon'' = \frac{i\sigma}{\varepsilon_0 \omega} \gg \varepsilon' \tag{12}$$

where ε_0 is the dielectric permittivity of vacuum. Therefore, in these two media $\delta \sim \pi/2$ and it is safe to assume that δ remains approximately constant within the gradual transition layer between the seabed and the seawater. Let us also assume that the large-scale roughness of the sandy seabed defines the width ξ of the σz transition layer. Under these assumptions, Eq. (11) may be rewritten as

$$V = -\frac{i\sigma\omega}{\varepsilon_0 c^2} - \frac{1}{2}\frac{\partial^2 \sigma}{\sigma \partial z^2} + \frac{3}{4}\frac{\left(\partial\sigma/\partial z\right)^2}{\sigma^2} \tag{13}$$

The effective potential energy defined by Eq. (13) is plotted in Fig. 2 for two different cases of seabed surface roughness and two different operating frequencies (note that in both cases $\mathrm{Im}(V) \ll \mathrm{Re}(V)$).

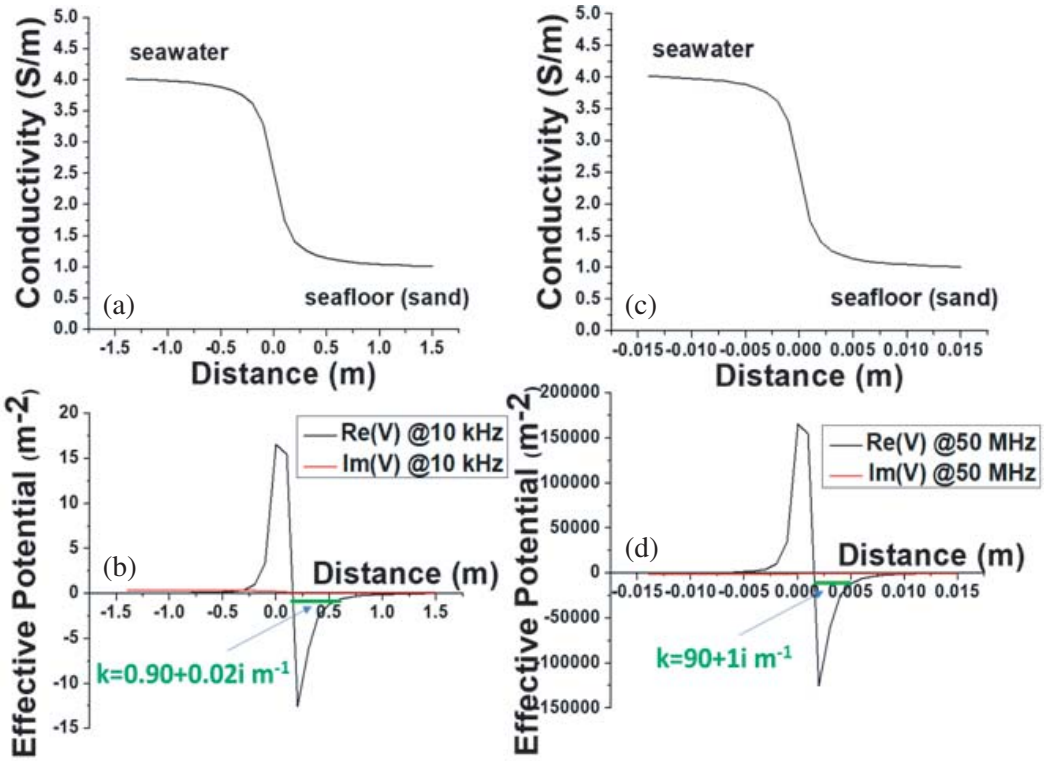

Figure 2. (a) Plot of an assumed seabed $\sigma(z)$ transition layer in which conductivity changes from σ_{water} to σ_{sand} within about 0.5 m. (b) The corresponding effective potential energy (both real and imaginary parts) at the water-seabed interface defined by Eq. (13) is plotted for the 10 kHz band. The numerically obtained effective energy level is shown in green. (c) A more abrupt $\sigma(z)$ transition layer in which conductivity changes from σ_{water} to σ_{sand} within about 5 mm. (d) The corresponding effective potential energy at the interface is plotted for the 50 MHz band. The numerically obtained effective energy level is shown in green.

In both cases, the conductivity of the transition region was assumed to follow a simple arctan law: $\sigma = A\arctan(z/\xi)+B$, where $A = (\sigma_{sand}-\sigma_{water})/\pi$ and $B = (\sigma_{sand}+\sigma_{water})/2$. The long-propagating-range eigenstate in both cases may be approximately determined using the virial theorem [18] as

$$k^2 \approx -\frac{\int_{-\infty}^{+\infty} \psi V(z)\psi * dz}{2\int_{-\infty}^{+\infty} \psi\psi * dz} \tag{14}$$

(due to almost $\sim 1/z$ functional behavior of $V(z)$ near the potential barrier, see Figs. 2(b), (d)). However, to obtain better precision, in this work the effective Schrodinger equation was solved numerically using the Numerov method [20]. This method is the most commonly used method to numerically solve ordinary differential equations of the second order in which the first-order term does not appear. The numerically obtained effective energy levels are shown schematically in green in Figs. 2(b) and (d). The wavelength of the resulting surface wave solution is $\lambda = 2\pi/k$, and $L = \mathrm{Im}(k)^{-1}$ defines the SEW propagation distance. Based on the numerical solution of the resulting Schrodinger equation, it appears that a 10 kHz radio signal propagation distance in the case considered in Figs. 2(a) and (b) reaches about $L \sim 50$ m, which has the same order of magnitude as the classical skin depth in wet sand and considerably exceeds the classical skin depth about 3 m at 10 kHz in seawater [18]. The surface wave propagation distance is about seven times larger than its wavelength computed numerically as $\lambda = 2\pi/k = 7$ m, which clearly indicates "propagating" characteristic ($\lambda \ll L$) of the surface wave. Using a good radio receiver, which is typically capable of operating down to at least ~ -100 dBm signal levels, should allow communication distances of the order of 500 m at 10 kHz along the sandy seabed. If a sharper transition region from σ_{water} to σ_{sand} of the order of 5 mm is assumed, the effective potential (shown in Fig. 2(d)) for the 50 MHz band gives rise to $\lambda = 2\pi/\mathrm{Re}(k) = 7$ cm at this frequency, and the corresponding propagation length $L = 1/\mathrm{Im}(k)$ equals about 1 m. Under these conditions, using a good radio receiver capable of operating down to ~ -100 dBm signal levels should allow communication distances of the order of 10 m along the sandy seabed.

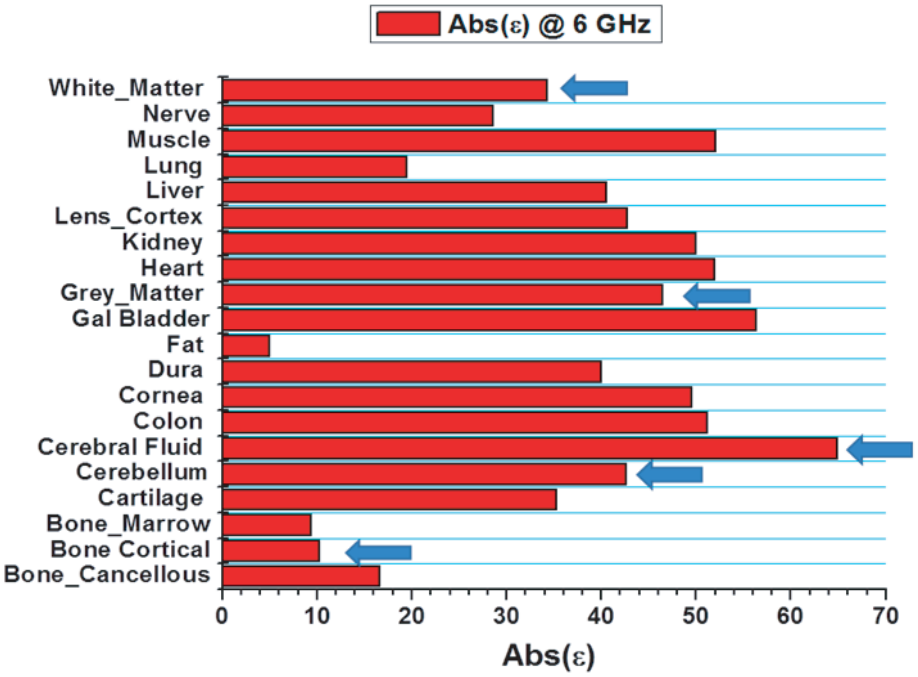

Figure 3. Magnitude of the dielectric permittivity of various human tissues at 6 GHz (based on the data assembled in [21]). Various tissues present in the head are indicated by arrows.

3.2. Surface Wave Propagation along Interfaces between Biological Tissues

Let us now consider SEW solutions which may exist at planar interfaces between different tissues inside a human body. As a general observation, commonly used FCC data on the dielectric parameters of various human body tissues [21] indicate that at 6 GHz the loss tangent variations between different tissues are not as pronounced as variations between the absolute magnitudes of ε. This observation is illustrated in Figs. 3 and 4. In particular, the loss angle only varies by about 0.015 between the skull bone and the grey matter, while the absolute magnitude of ε varies by approximately factor of 4.5 between these tissues. This observation indicates that under right conditions SEWs may be excited and guided by many various tissue boundaries inside a human body. As a proof of principle demonstration, in order to avoid unnecessary complications, let us consider an idealized geometry in which a planar skull bone is separated from the grey matter tissue by a 0.5 mm thick transition layer, in which the loss angle δ remains approximately constant at 6 GHz, as illustrated in Fig. 5(a). The thickness of the transition region was chosen based on the lattice-like appearance of the bones of the cranial vault with a typical scale of the order of 500 μm — see for example Fig. 3 from [22] (note also that the bone-tendon junctions also have similar transition layer thicknesses — see Fig. 5 from [23]). Once again, the dielectric permittivity of the transition region was assumed to follow a simple arctan law: $\varepsilon = A\arctan(z/\xi) + B$, where $A = (\varepsilon_{grey}\varepsilon_{bone})/\pi$ and $B = (\varepsilon_{grey}+\varepsilon_{bone})/2$. A SEW solution having $\mathrm{Im}(k) \ll \mathrm{Re}(k)$ does appear in this case, and it is indicated by the green line in Fig. 5(b). Potential effects of SEW excitation and propagation along such an interface are illustrated in Fig. 6, which depicts numerical simulations of surface wave excitation by a 6 GHz point source located at different distances from the interface. In order to illustrate the effects of SEW scattering, a 0.4 mm diameter metal particle has been placed inside the transition layer. A pattern of standing surface waves appears in Figs. 6(a) and (b), which corresponds to $\lambda \sim 3$ mm and $\mathrm{Re}(k) \sim 1.7 \times 10^3\ \mathrm{m}^{-1}$ (which is consistent with the results of direct calculations shown in Fig. 5(b)). These simulations indicate that the deeply subwavelength effective SEW waveguide, which is formed by the transition layer, only gets excited when the point source is placed in the immediate vicinity of the transition layer. The SEW is not excited when the point source is separated by more than ~ 1 mm from the transition layer. While this result is encouraging from the EM radiation safety prospective, simulations depicted in Fig. 7 look much less reassuring. In these simulations, a SEW cavity is formed within the same transition layer as in Fig. 6 by placing two 0.4 mm diameter cylindrical metal scatterers inside the layer, separated by 2 mm, which approximately equals

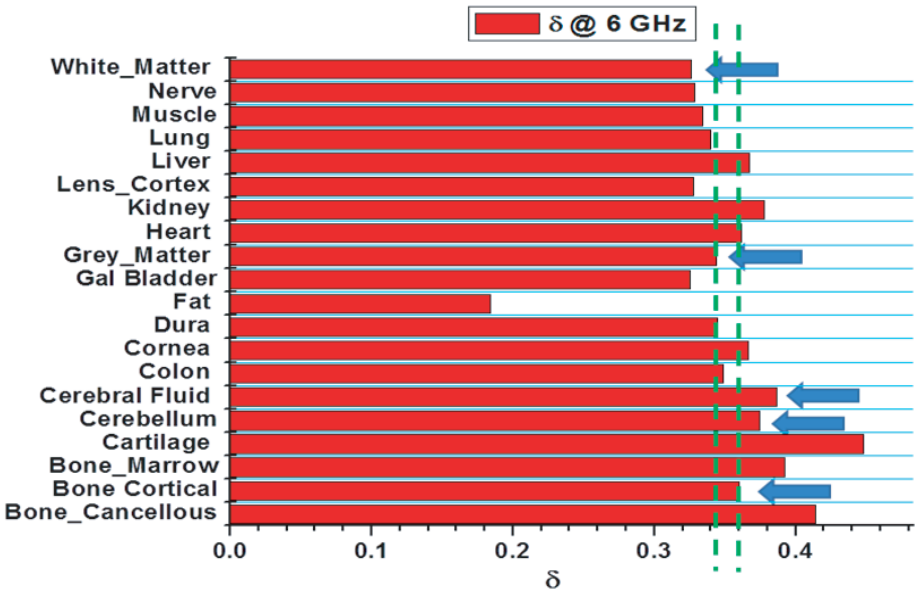

Figure 4. Loss angle of various human tissues at 6 GHz (based on the data assembled in [21]). Various tissues present in the head are indicated by arrows. The green dashed lines indicate difference of the loss angle between the skull bones and the grey matter.

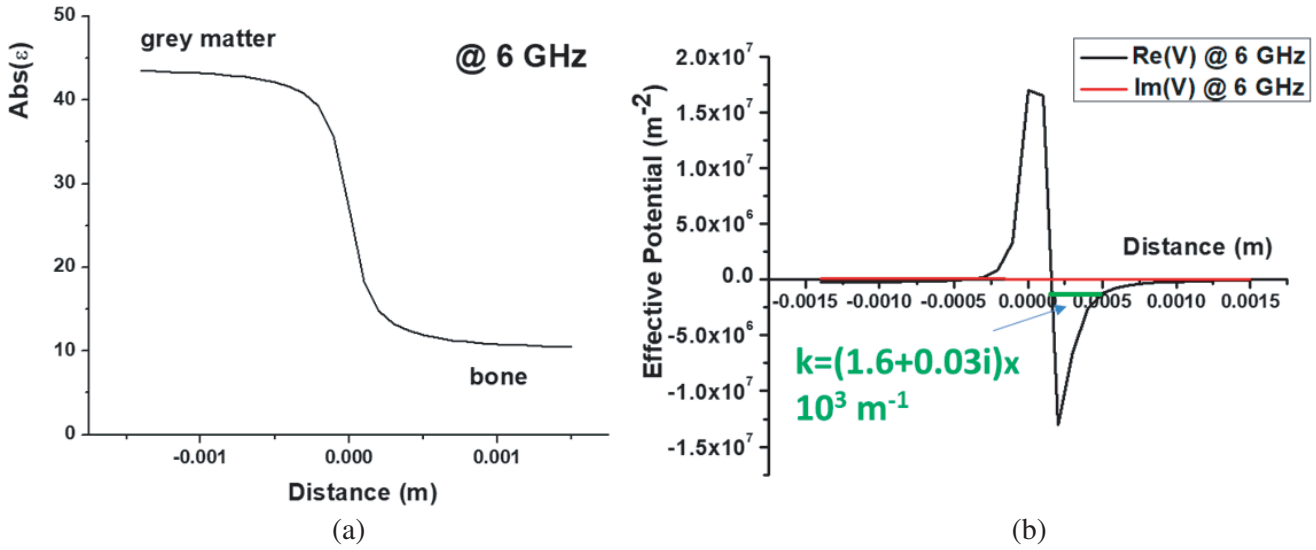

Figure 5. (a) Plot of an assumed transition layer in which the magnitude of the dielectric permittivity changes from its value in the skull bone to its value in the grey matter within about 0.5 mm. (b) The corresponding effective potential energy (both real and imaginary parts) at the interface defined by Eq. (11) is plotted for the 6 GHz band. The numerically obtained effective energy level is shown in green.

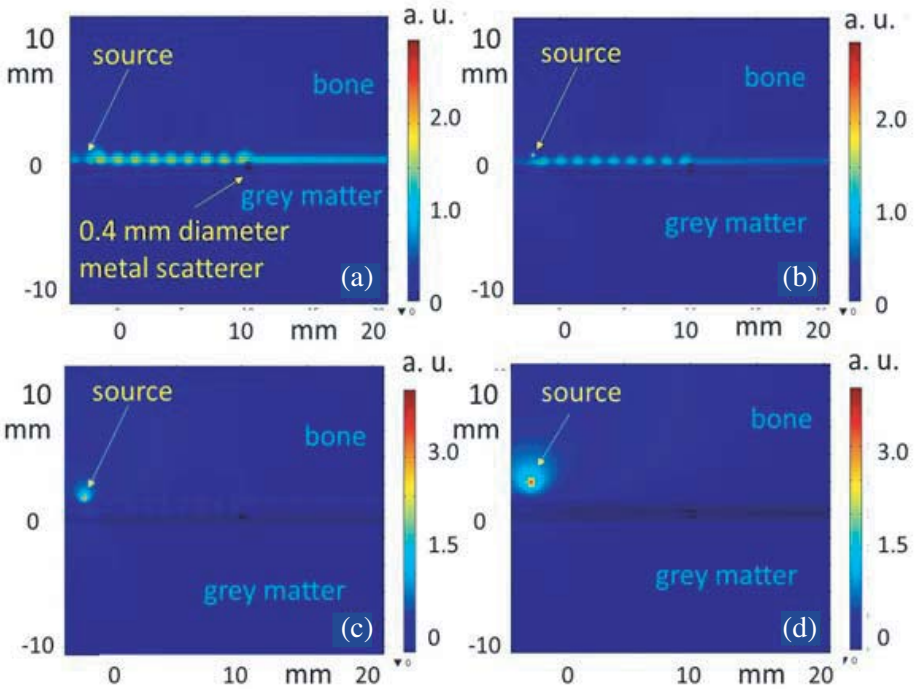

Figure 6. Simulations of surface wave excitation and scattering in the transition layer between the skull bone and the grey matter at 6 GHz. The SEW electric field images are 25 mm × 25 mm. The distance between an excitation source and the transition layer increases progressively from (a) to (d). The SEW is excited by a 6 GHz point source only when the source is placed within about 1 mm from the interface. The RF field in the effective SEW waveguide is scattered by a 0.4 mm diameter metal particle placed inside the waveguide.

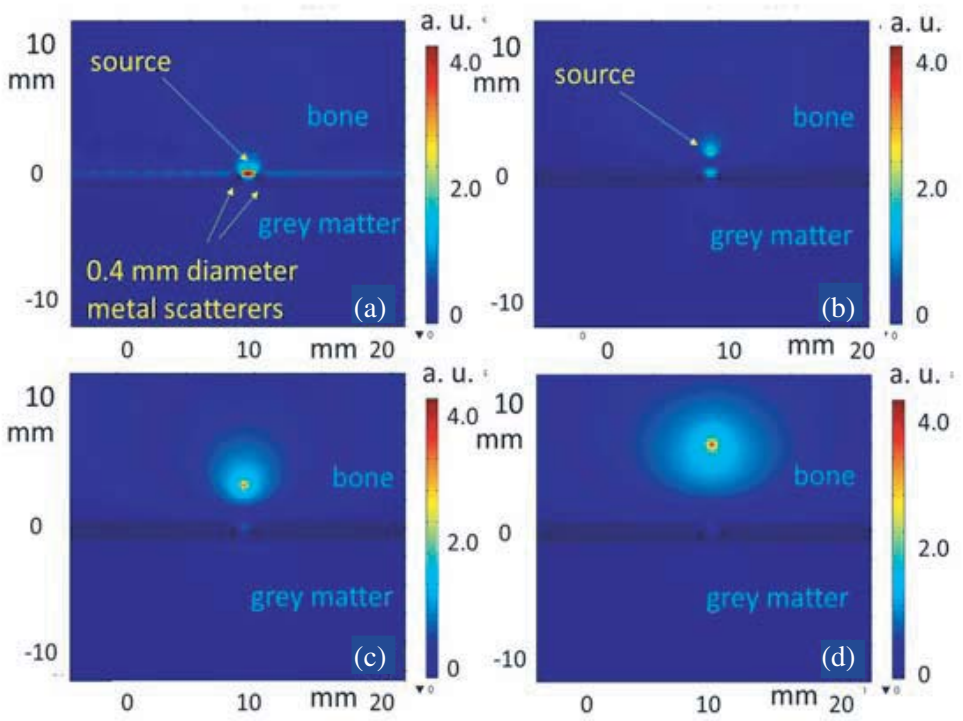

Figure 7. Simulations of a SEW cavity excitation by a 6 GHz point source positioned at different distances from the interface. The distance between an excitation source and the interface increases progressively from (a) to (d). The SEW electric field images are 25 mm × 25 mm. The SEW cavity is formed by two 0.4 mm diameter cylindrical metal scatterers placed within the transition layer at half SEW wavelength (2 mm) from each other. Under such circumstances the SEW cavity is excited rather efficiently even if the distance between the cavity and the point source reaches centimeter-scale distances.

one half of the SEW wavelength at 6 GHz (note that the SEW wavelength is much smaller than the free space wavelength at 6 GHz). As can be seen from Fig. 7, under such circumstances the SEW cavity is excited rather efficiently even if the distance between the cavity and the point source reaches centimeter-scale distances.

Table 1. Comparison of basic properties of different surface electromagnetic wave solutions.

surface wave type	bounding media	interface sharpness	wavelength range
surface plasmon	metal-dielectric	sharp	from ∼ free space to deep subwavelength
Zenneck wave	lossy conductor-dielectric	sharp	∼ free space
interfacial wave	lossy conductor-lossy conductor	gradual	deep subwavelength

4. CONCLUSION

I have demonstrated that a new kind of low loss propagating surface electromagnetic wave, an "interfacial wave", may exist at a gradual interface between two lossy conductive media. The comparison of its properties with the more well-known surface electromagnetic wave solutions, such as surface plasmons

and Zenneck waves is summarized in Table 1. Such a deep-subwavelength surface wave may be guided by a seafloor-seawater interface, and it may be used in radio communication and imaging underwater. Similar surface waves may also be guided by various tissue boundaries inside a human body. For example, such surface wave solutions may exist at planar interfaces between skull bones and grey matter inside a human head at 6 GHz. A possibility of deep sub-wavelength SEW cavities (or "hot spots") has been revealed in numerical simulations of SEW-related effects in human tissues. Therefore, it will be important to reexamine EM radiation safety issues associated with the potential excitation and scattering of the newly discovered surface electromagnetic waves inside a human body.

ACKNOWLEDGMENT

This work was supported in part by DARPA/AFRL Award FA8650-20-C-7027.

REFERENCES

1. Rayleigh, L., "On waves propagated along the plane surface of an elastic solid," *Proceeding of the London Mathematical Society*, Vol. s1-17, No. 1, 4–11, 1885.
2. Sommerfeld, A. N., "Propagation of waves in wireless telegraphy," *Annalen der Physik*, Vol. 28, 665–737, 1909.
3. Love, A. E. H., "Some problems of geodynamics," *Nature*, Vol. 89, 471–472, 1912.
4. Wait, J. R., "Launching a surface wave over the earth," *Electronics Letters*, Vol. 3, No. 9, 396–397, 1967.
5. Schelkunoff, S. A., *Electromagnetic Waves*, D. Van Nostrand Company, Inc., New York, NY, 1943.
6. Collin, R. E., *Field Theory of Guided Waves*, IEEE Press-Wiley, New York, NY, 1991.
7. Zayats, A. V., I. I. Smolyaninov, and A. Maradudin, "Nano-optics of surface plasmon-polaritons," *Physics Reports*, Vol. 408, 131–314, 2005.
8. Oruganti, S. K., F. Liu, D. Paul, J. Liu, J. Malik, K. Feng, H. Kim, Y. Liang, T. Thundat, and F. Bien, "Experimental realization of Zenneck type wave-based non-radiative, non-coupled wireless power transmission," *Scientific Reports*, Vol. 10, 925, 2020.
9. Alibakhshikenari, M., B. S. Virdee, P. Shukla, C. H. See, R. A. Abd-Alhameed, F. Falcone, and E. Limiti, "Improved adaptive impedance matching for RF front-end systems of wireless transceivers," *Scientific Reports*, Vol. 10, 14065, 2020.
10. Limiti, E., F. Falcone, R. A. Abd-Alhameed, B. S. Virdee, M. Alibakhshikenari, and C. H. See, "Impedance matching network based on metasurface (2-D metamaterials) for electrically small antennas," *2020 IEEE International Symposium on Antennas and Propagation and North American Radio Science Meeting (2020 IEEE AP-S/URSI)*, 1953–1954, Montréal, Canada.
11. Alibakhshikenari, M., B. S. Virdee, C. H. See, R. A. Abd-Alhameed, F. Falcone, and E. Limiti, "Metasurface for controlling polarization of scattered EM waves," *4th Australian Microwave Symposium*, Sydney, Australia, 2020.
12. Alibakhshikenari, M., B. S. Virdee, C. H. See, R. A. Abd-Alhameed, F. Falcone, and E. Limiti, "Automated reconfigurable antenna impedance for optimum power transfer," *2019 IEEE Asia-Pacific Microwave Conference (APMC)*, 1461–1463, Singapore, 2019.
13. Alibakhshikenari, M., B. S. Virdee, C. H. See, R. A. Abd-Alhameed, F. Falcone, and E. Limiti, "Energy harvesting circuit with high RF-to-DC conversion efficiency," *2020 IEEE International Symposium on Antennas and Propagation and North American Radio Science Meeting (2020 IEEE AP-S/URSI)*, 1299–1300, Montréal, Canada, 2020.
14. Alibakhshikenari, M., et al., "Impedance bandwidth improvement of a planar antenna based on metamaterial-inspired T-matching network," *IEEE Access*, Vol. 9, 67916–67927, 2021.
15. Alibakhshikenari, M., et al., "A comprehensive survey of metamaterial transmission-line based antennas: Design, challenges, and applications," *IEEE Access*, Vol. 8, 144778–144808, 2020.

16. Alibakhshikenari, M., et al., "A comprehensive survey of various decoupling mechanisms with focus on metamaterial and metasurface principles applicable to SAR and MIMO antenna systems," *IEEE Access*, Vol. 8, 192965–193004, 2020.
17. Smolyaninov, I. I., Q. Balzano, C. C. Davis, and D. Young, "Surface wave based underwater radio communication," *IEEE Antennas and Wireless Propagation Letters*, Vol. 17, 2503–2507, 2018.
18. Landau, L. D. and E. M. Lifshitz, *Quantum Mechanics: Non-relativistic Theory*, Vol. 3, No. 45, Elsevier, 2013.
19. Müller, H., T. von Dobeneck, C. Hilgenfeldt, B. SanFilipo, D. Rey, and B. Rubio, "Mapping the magnetic susceptibility and electric conductivity of marine surficial sediments by benthic EM profiling," *Geophysics*, Vol. 77, 1JF-Z19, 2012.
20. Numerov, B. V., "A method of extrapolation of perturbations," *Monthly Notices of the Royal Astronomical Society*, Vol. 84, 592–601, 1924.
21. http://www.fcc.gov/general/body-tissue-dielectric-parameters.
22. Richtsmeier, J. T. and K. Flaherty, "Hand in glove: Brain and skull in development and dysmorphogenesis," *Acta Neuropathol.*, Vol. 125, 469–489, 2013.
23. Wong, M. W. N., L. Qin, K. M. Lee, and K. S. Leung, "Articular cartilage increases transition zone regeneration in bone-tendon junction healing," *Clin. Orthop. Relat. Res.*, Vol. 467, 1092–1100, 2009.